Hardware-in-the-Loop Experimental Setup of a LCL-Filtered Grid-Connected Inverter with Digital Proportional-Resonant Current Controller

Hardware-in-the-Loop Experimental Setup of a LCL-Filtered Grid-Connected Inverter with Digital Proportional-Resonant Current Controller

Tiago Davi Curi Busarello
Department of Engineering
Federal University of Santa Catarina
Blumenau, Brazil
tiago.busarello@ufsc.br

Joel Filipe Guerreiro
School of Electrical and Computer Engineering
University of Campinas
Campinas, Brazil
joel.engeletrica@gmail.com

Marcelo Godoy Simões
Electrical Engineering Department
University of Vaasa
Vaasa, Finland
mgsimoes@ieee.org

José Antenor Pomilio
School of Electrical and Computer Engineering
University of Campinas
Campinas, Brazil
antenor@dsce.fee.unicamp.br

***Abstract*—This paper presents a Hardware-in-the-Loop setup of a LCL-filtered grid-connected inverter with digital Proportional-Resonant current controller. The power structure of the system, i.e. the power DC source, the transistor-based inverter, the LCL filter, the sensors and the grid are emulated in the Real-Time Simulator HIL402 from Typhoon-HIL, while the control strategy is embedded in the Digital Signal Controller TMS320F28335 from Texas Instruments. Descriptions of how to design the PR controller is presented. Details about the settings of the RTS are also described. The HIL verification consists of applying several real time test cases along the power structure as well as in the control strategy, allowing designers to rapidly evaluate the efficacy of the PR controller. Some modifications are: inclusion of an oscillation at the DC-link voltage, frequency variation at the grid voltage, variation of grid impedance, current reference step, among others. Results show that the HIL verification is an attractive tool for evaluating the PR current controller of a LCL-filtered grid-connected inverter.**

***Index Terms*—hardware-in-the-loop, proportional-resonant, digital controller, DC-AC converter.**

I. Introduction

A Hardware-in-the-Loop (HIL) setup is a combination of a Real-Time Simulator (RTS) and a control system usually implemented by a microcontroller, a Digital Signal Controller (DSC) or by a Digital Signal Processor (DSP). The connection of the control system and the RTS may be direct or through an interface board, depending on the voltage compatibility of their terminals. The RTS simulates a system in real time frame and generates waveforms that describe the modeled system. The control system receives these waveforms, process its control algorithm and send back to the RTS an actuator signal like a PWM or a command signal. In this way, the modeled and the control systems interact each other in a loop. A HIL setup can also be made by connecting several RTS and several control systems in a single setup structure [1].

The HIL technology has been showing a lot of promises for industries and academia due to its ability to approach a risk-free device and an accelerated prototyping method in developing researches in the field of engineering. For example, designers can test a new control law in an aircraft system through a HIL, in one hand avoiding tinkering in a real system, which would be technically infeasible because of safety reasons.In [2], the authors verified a three-phase modular multilevel converter in a HIL setup. The setup comprises seven RTS and external logical cards. A total of 192 transistors were emulated in the seven RTS. The authors in [3] presented an implementation of stationary and synchronous frame current regulators for grid tied inverter using Typhoon HIL System. A protective relay upgrade utilizing RTS technology is proposed in [4]. In such a case, the papers covers an application of RTS technology for the development, testing, training, and execution of a 5-kV main–tie–main intelligent electronic device. Other relevant publications covering HIL setups may be found in [5]–[9].

HIL testing is also an interesting approach to evaluate Grid-Connected Inverter (GCI) applications. In the recent years, a great number of power generating sources, such as such as photovoltaic, storage and wind turbines were connected to the distribution grid through a GCI [10], [11]. For single-phase GCI applications, the Proportional-Resonant (PR) current controller is widely used. A variety of methodologies guides the designer to accurately employ PR controllers in applications covering GCIs. In [12] the authors designed a PR controller with multiple resonant harmonic compensators for grid-connected PV systems. In such a case, the strategy

This work was financially supported by the National Council for Scientific and Technological Development (CNPq), grant #303859/2020-2, Sao Paulo Research Foundation (FAPESP), grant #2016/08645-9.

also has the fault ride trough feature. In [13] the design of the parameters are obtained in a straightforward way. An optimization and implementation of the PR controller for GCI with significant computation delay is presented in [14]. The delay may be compensated using a scheme with trigonometric functions. In [15] the authors presented a step-by-step procedure for LCL-type single-phase GCI using digital PR controller With capacitor-current feedback. Authors also have exploited the impedance-based stability properties of PR controllers in microgrids [16], [17]. The books [18], [19] have interesting approaches for designing PR current controllers.

This paper presents a HIL verification of a LCL-filtered GCI with digital PR current controller. The main contributions of this paper are: *i*: supply an overview of a HIL setup in verifying a power electronic application and *ii*: design a digital PR-based current controller for LCL-filtered GCI in a simplified manner. The verification consists of applying changes along the system parameters to evaluate the efficacy of the designed PR controller. The HIL setup comprises the RTS HIL402 and DSC TMS320F28335. Section II gives descriptions of the system. In Section III, the steps to design the digital PR current controller is carefully presented. Information of the HIL setup as well as its verification are given in Section IV. Section V concludes the paper.

II. System Description

Fig. 1 presents a simplified block diagram of the HIL setup. The dashed board named as **A** shows the power structure. It has a DC source, a full-bridge inverter, a LCL filter and the grid source and impedance. The LCL filter is made by the converter-side inductor (L_1), the grid-side inductor (L_2). the capacitor (C_1) and the passive-damping resistor (R_d). These elements are not shown in the figure. The inverter output current (i_{out}) and the PCC voltage (v_{PCC}) are outputted and sent to the DSC through the interface board. The dashed board named as **B** shows the control strategy. The inverter output current (i_{out}) is compared to the current reference signal ($i_{out}*$). The resulting signal goes to the PR controller, which in turn, acts in the pulse width modulator.

The PR controller consist of the proportional gain (k_p), the resonant gain (k_i) and a digital resonant filter ($H(z)$). The strategy uses the PWM to command the transistors. The variable k is a scale-factor and its value should be chosen to make a tiny adjustment in the controller due to the fact that the grid impedance is unknown and not taken into account in the PR design. Its value is obtained empirically by observing the simulation results. The PCC voltage (v_{PCC}) is used in the control strategy to generate the current reference signal. This is obtained by a Phase-Locked Loop algorithm [20] (not shown in the figure). It is worth noting that there is no feed-forward action in this control strategy. Moreover, the DC-link has a fixed voltage supplied by a DC source. The control strategy runs in per-unit, normalized at the maximum output current. A host PC is used to draw the model of the HIL402 and the oscilloscope is for collecting results at the HIL402 analog outputs.

III. Designing the Digital Current Controller

The procedure for designing a digital PR current controller is divided into three parts: (i) computing the proportional gain (k_p); (ii) computing the resonant gain (k_i) and (iii) designing a digital resonant filter which is described by the transfer function ($H(z)$).

The proportional and resonant gains are obtained by the Naslin Polynomial Method, also known as normal polynomials with adjustable damping. A detailed description of this methods is beyond the scope of this paper, but it can be found in [18].

The proportional and resonant gains are then given by:

$$k_p = \frac{(2\xi+1)(\sqrt{(2\xi+1)}\omega_r L_{eq} - R_{eq}}{V_{dc}h_i} \tag{1}$$

$$k_i = \frac{w_r^2 L_{eq}[(2\xi+1)^2 - 1]}{2V_{dc}h_i} \tag{2}$$

The following statements point out important features for previous equations:

- L_{eq} means the sum of the inductances of the LCL filter. Therefore, $L_{eq} = L_1 + L_2$.
- R_{eq} means the sum of the resistances of the inductors of the LCL filter. Therefore, $R_{eq} = R_1 + R_2$.
- h_i is the current sensor gain.
- ξ is the damping factor and its value must be in the range of 0 and 1. A value between 0.5 and 1 is a good choice.
- The computation of the proportional and resonant gains does not take into account the capacitance of the LCL filter. As a result, the LCL filter was approximated by a L filter with L_{eq} inductane. Depending on the values of the LCL elements, such approximation is valid, as described in [21] and also in the Fig. 2. Note that for low frequencies the behavior of the LCL and the L filters is the same. The values used in this chart are those presented in Tab. I, that are the parameters of the system used in this paper.
- ω_r is the angular resonant frequency. Such a frequency is chosen to be the same of the grid voltage.
- The time delay of digital controllers is not considered in this design. As will be demonstrated later, the non consideration of the delay is valid for the system under study. However, the scheme presented in [14] would be an option for taking into account the delay effect.

The last part is designing the digital resonant filter. Its procedure is a discrete approximation of a continuous-time band-pass filter. The transfer function of the continuous-time resonant filter is given by:

$$H(s) = \frac{B_r s}{s^2 + 2\zeta B_r s + w_r^2} \tag{3}$$

where B_r is the resonant bandwidth and ζ is the damping factor. It is worth noting that this damping factor is different from that used in computing the proportional and resonant gains. Another important point is that the resonant gain is already computed in (2) and is not used here. The value of

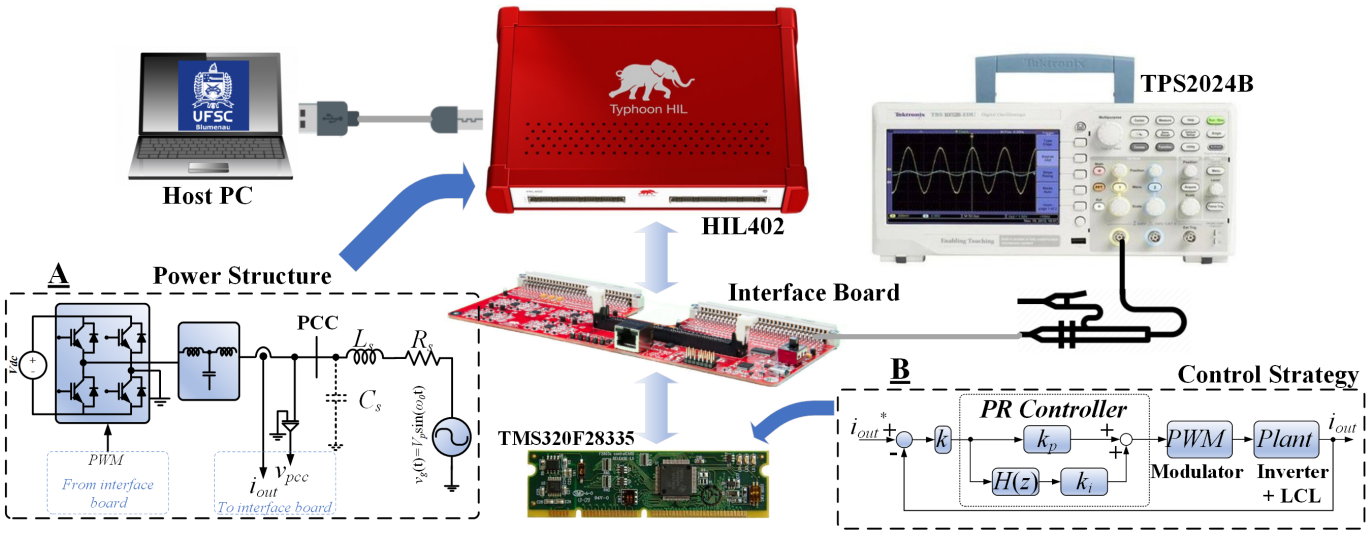

Fig. 1. Simplified block diagram of the HIL setup.

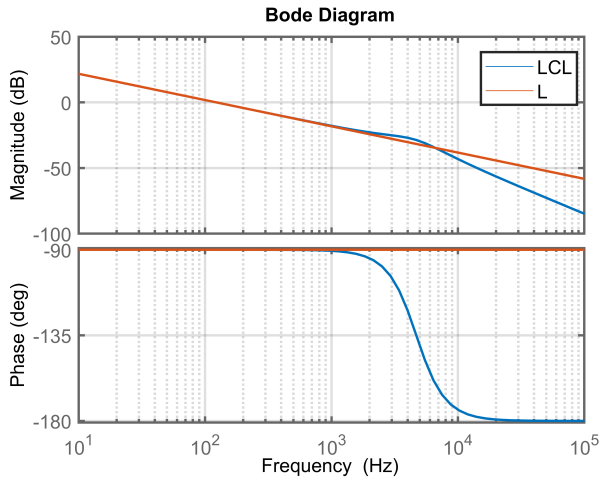

Fig. 2. Frequency response for the LCL and L filters.

B_r should be a few Hertz and ζ any value between 0.1 and 1. By choosing $\zeta = 0.5$ makes the resonant filter to present $0dB$ at the resonant frequency, as will be demonstrated later. Therefore, such a choice is adopted in the following procedure. The digital resonant filter is then obtained by:

$$H(z) = Z\{H(s)\} = \frac{b_0 + b_1 z^{-1} + b_2 z^{-2}}{a_0 + a_1 z^{-1} + a_2 z^{-2}} \tag{4}$$

where $Z\{\cdot\}$ means the Z-transform and it is computed by its original definition [22]. By defining ω as:

$$\omega = \sqrt{\omega_r^2 - 0.25B_r^2} \tag{5}$$

one can write (3) as:

$$H(s) = B_r \frac{s + 0.5B_r}{(s + 0.5B_r)^2 + w^2} - \frac{0.5B_r^2}{w} \frac{w}{(s + 0.5B_r)^2 + w^2} \tag{6}$$

The purpose of writing $H(s)$ as shown in (5) is to ease using the following pair of equations brought from the Z-transform table.

$$\frac{\omega}{(s+a)^2 + w^2} \Leftrightarrow \frac{e^{-aT} z^{-1} sin(\omega T)}{1 - 2e^{-aT} z^{-1} cos(\omega T) + e^{-2aT} z^{-2}} \tag{7}$$

$$\frac{s+a}{(s+a)^2 + w^2} \Leftrightarrow \frac{e^{-aT} z^{-1} cos(\omega T)}{1 - 2e^{-aT} z^{-1} cos(\omega T) + e^{-2aT} z^{-2}} \tag{8}$$

where T is the sampling period.

Using (7) and (8) in (4), the coefficients of the digital resonant filter is given by:

$$b_0 = B_r T \tag{9}$$

$$b_1 = (-B_r e^{-0.5B_r T} cos(T\sqrt{\omega_r^2 - 0.25B_r^2} - \psi))T \tag{10}$$

$$b_2 = 0 \tag{11}$$

$$a_0 = 1 \tag{12}$$

$$a_1 = -2e^{-0.5B_r T} cos(T\sqrt{\omega_r^2 - 0.25B_r^2}) \tag{13}$$

$$a_2 = e^{-B_r T} \tag{14}$$

where

$$\psi = \frac{0.5B_r^2}{\sqrt{\omega_r^2 - 0.25B_r^2}} e^{-0.5B_r T} sin(T\sqrt{\omega_r^2 - 0.25B_r^2}) \tag{15}$$

The T in (9) and (10) was included to compensate the process of sampling.

TABLE I
SYSTEM PARAMETERS

Parameters	Value
Grid Voltage (peak)	$V_{Apk} = 180\,V$
Grid frequency	$f = 60\,Hz$
Grid resistance	$R_s = 0.1\,\Omega$
Grid inductance	$L_s = 1.5\,mH$
Inverter nominal power	$P_{nom} = 1.5\,kW$
DC-Bus voltage	$Vdc = 225\,V$
Current sensor gain	$h_i = 1/10$
Converter-side inductance	$L_1 = 1\,mH$
Resistance of L_1	$R_1 = 0.1\,\Omega$
Grid-side inductance	$L_2 = 300\,uH$
Resistance of L_1	$R_2 = 0.1\,\Omega$
LCL capacitor	$C_1 = 5\,uF$
LCL damping resistor	$R_d = 6.8\,\Omega$
Switching frequency	$f_{sw} = 24\,kHz$
Sampling frequency	$f_s = 24\,kHz$
Damping factor	$\xi = 0.975$
Resonant bandwidth	$B_r = 9.4247\,rad/s$
Resonant frequency	$w_r = 2\pi 60\,rad/s$
Scale-factor	$k = 3$

TABLE II
PARAMETERS OF THE DESIGNED PR CONTROLLER

Parameters	Value
Proportional gain	$k_p = 0.101474487082548$
Resonant gain	$k_i = 31.624581206146559$
b_0	0.000392699081698
b_1	-0.000392650641728
b_2	0
a_0	1
a_1	-1.999360691417785
a_2	0.999607378014494

IV. HARDWARE-IN-THE-LOOP SETUP AND VERIFICATION

The power structure presented in Fig. 1 is emulated in the HIL402 while the control strategy is executed within the TMS320F28335. The interface board *HIL-DSP-100-Interface* from Typhoon is used to connect the DSC to the HIL402. The interface board has offset and amplitude adjustments to make the signals compatible with the microcontroller. Tab. I presents the parameters of the system.

After following the procedure of section III, the parameters of the designed PR controller are presented in Tab. II.

Fig. 3 presents the frequency response for the digital resonant filter ($H(z)$) as well as for the continuous-time resonant filter $H(s)$. The region of coincidence of the responses is large, indicating that the applied discrete approximation is adequate. The response of the digital resonant filter is $0\,dB$ at $60\,Hz$. For all other frequencies, the resonant filter attenuates the input signal. This behavior is expected and desired since the input signal of the PR controller is the error signal.

As previously mentioned, the effect of the natural delay due to digital employment was not considered in the equations of the proposed PR current controller. Fig. 4 presents Bode diagrams for open-loop transfer function with the designed controller and with and without considering the effect of the delay. For the sake of simplicity, these Bode diagrams were plotted in s-domain. The delay was modeled using Padè's approximation [23]. The delay has no effect on the magnitude

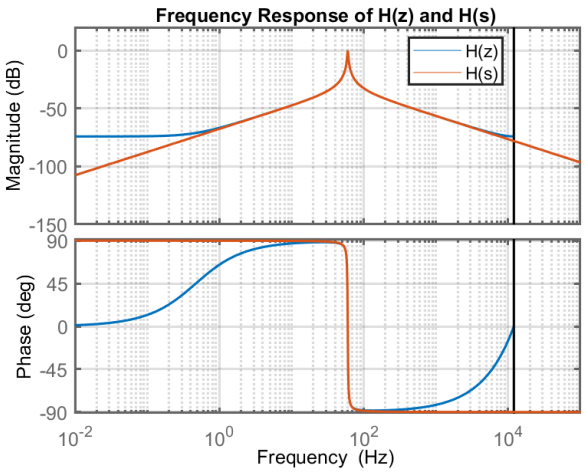

Fig. 3. Frequency response of $H(z)$ and $H(s)$.

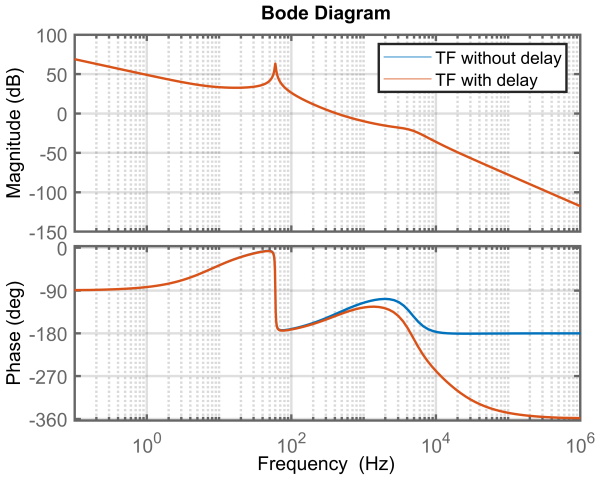

Fig. 4. Bode diagrams for open-loop transfer function with the designed controller and with and without considering the effect of the delay.

responses, since they were coincident. For the phase responses, the delay starts causing effects around $1\,kHz$. At $60\,Hz$, the delay has negligible effect.

For the proper operation of the HIL setup as well as the ability to evaluate the system under real-time changes, a panel must be created in the RTS software. Fig. 5 presents the panel created for evaluation of the HIL setup. The panel has some widgets for monitoring the RMS current and voltage as well as to visualize waveforms of variable along the power structure. The panel also allows the designer to change several parameters, such as grid voltage, frequency and angle, DC-link voltage and inverter output current. It is possible to include oscillation at the DC-link voltage and harmonics on the grid-voltage. This panel is also the location where the designer must include the sensors gains of the power structure.

For the following results, the variables presented are: PCC voltage (v_{PCC}), inverter output current (i_{out}), reference sig-

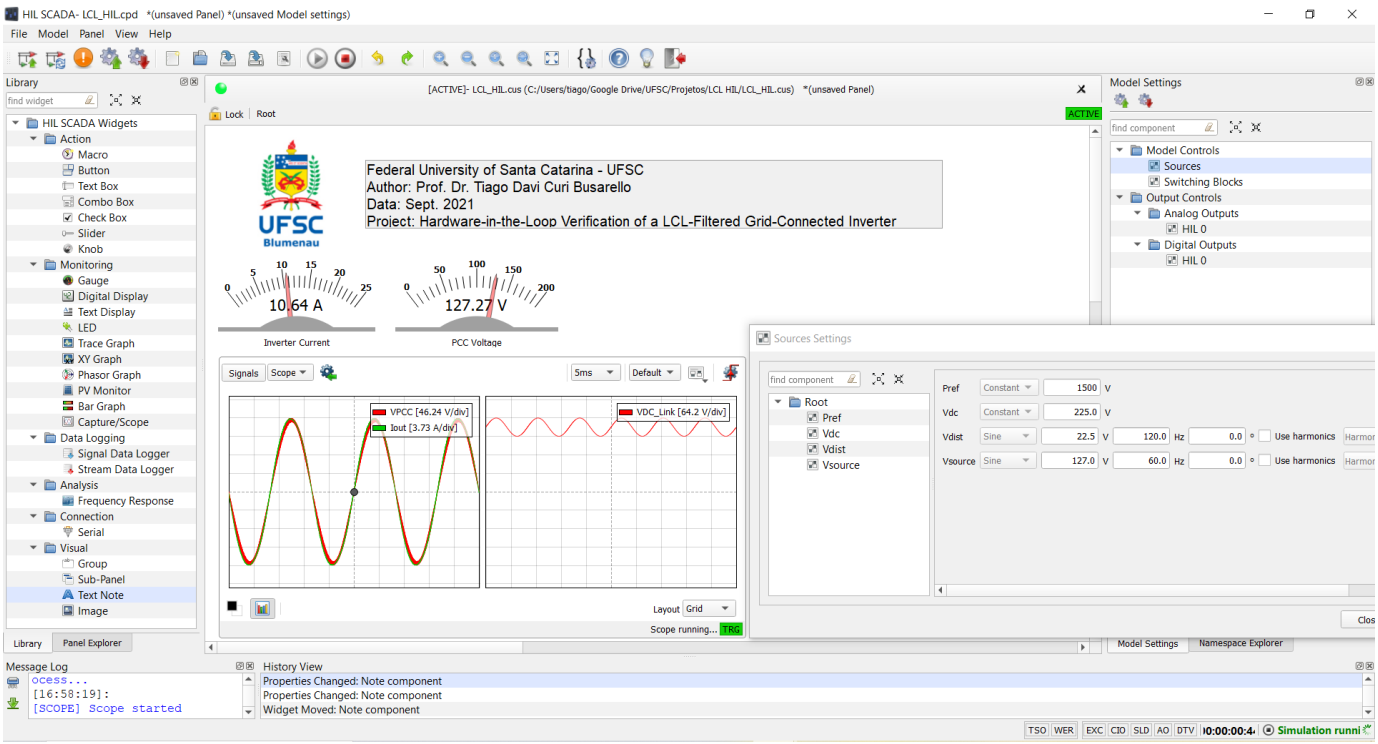

Fig. 5. Panel created for evaluation of the HIL setup.

nal for the inverter output current ($i_{out}*$) and the DC-link voltage (v_{dc}). Furthermore, the scales for the oscilloscope channels are: Ch1:180V/div, Ch2:225V/div. Ch3:10A/div and Ch4:10A/div). To sample the current reference signal which is within the DSC a 12-bit Digital-to-Analog Converter (DAC) is used.

Fig. 6 shows the behavior of the system during the initialization process. Initially, the current reference signal ($i_{out}*$) as well as the inverter output current (i_{out}) are null. Suddenly, the current reference signal changes to a sinusoidal waveform corresponding to an injected active power of $1500W$. The inverter output current rapidly follows the reference signal without large oscilations. At steady-state regime, the error is negligible. The PCC voltage was not compromised due to the operation of the inverter.

Fig. 7 presents the behavior of the system under a step-down at the current reference signal. The step is equivalent to a change in the injected active power from $1500W$ to $750W$ while Fig. 8 indicates the behavior under an inversion of the current reference signal. An inversion in the current reference signal means that the inverter passes to absorb active power from the grid. For both cases, the inverter output current keeps following the reference signal without considerable error after the transitions. For the second case, the transition was more severe due to the power flow inversion.

Fig. 9 depicts the behavior of the system at the moment of appearance of oscillation at the DC-link voltage. The oscillation has 22.5V and 120Hz. The inverter output current does not neither notice the occurrence of such an oscillation.

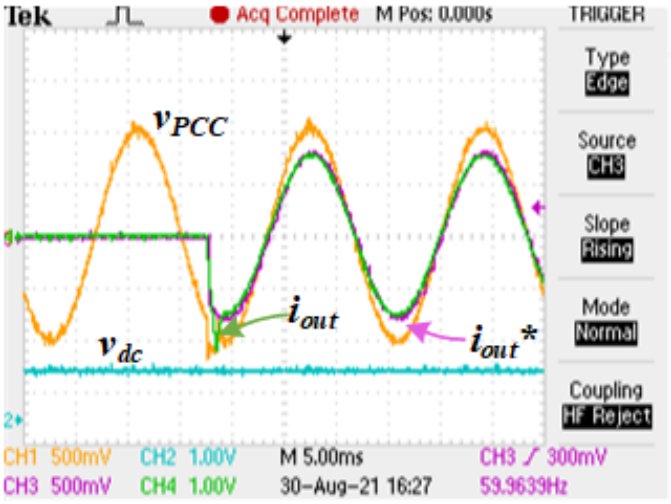

Fig. 6. Behavior of the system during the initialization process.

This shows the ability of the designed PR controller to work under such disturbance.

Fig. 10 presents the steady-state regime of the system when the grid frequency is $50\,Hz$. Even though such a change in the frequency may not happen in a real system, this was done as a test in order to verify the behavior of the designed PR controller. The result shows that the PR controller keeps working in such a situation, although a small phase-lag is introduced.. It is worth noting that the PLL contributes to keep the system working properly. Moreover, such a test ensures the

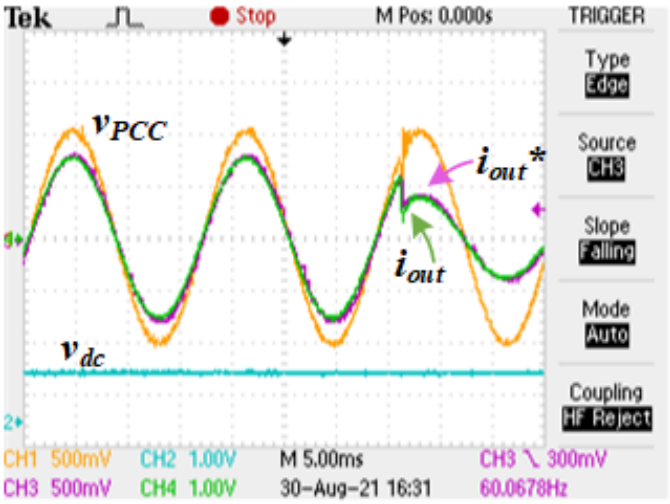

Fig. 7. Behavior of the system under a step-down at the current reference signal.

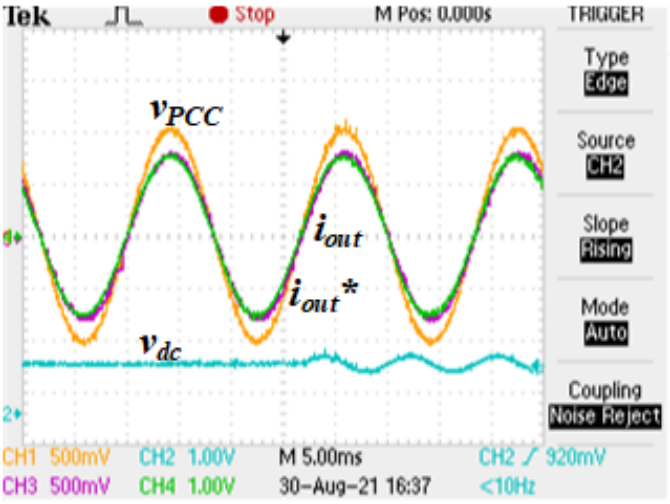

Fig. 9. Behavior of the system at the moment of appearance of oscillation at the DC-link voltage.

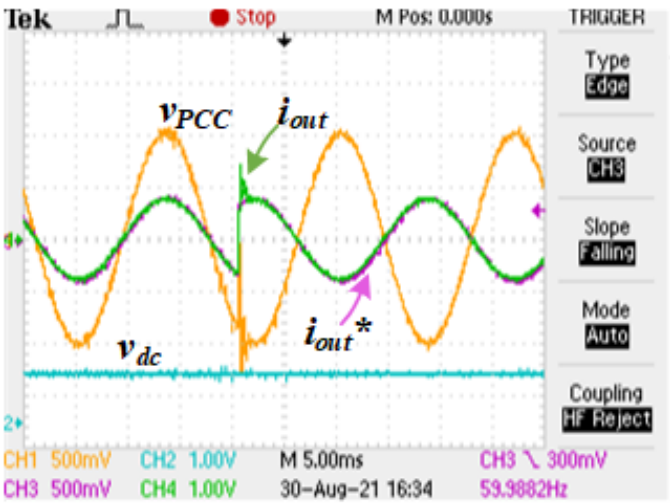

Fig. 8. Behavior of the system under an inversion of the current reference signal.

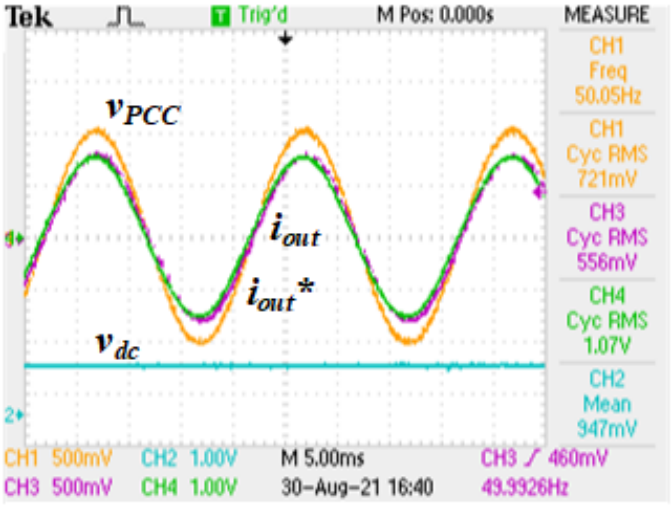

Fig. 10. Steady-state regime of the system when the grid frequency is 50 Hz.

ability of the PR controller to work satisfactorily when the grid frequency changes its value near to 60 Hz

Fig. 11 presents the steady-state behavior of the system when the PCC voltage has harmonic distortions. The PCC voltage has 5% at 5th and 1% at 7th components. The inverter output current keeps sinusoidal and following its reference signal with negligible error. In this case, the PLL also has its merit.

Fig. 12 and Fig. 13 both show results when the system has different grid impedance from those used in the previous tests. For 12, the grid impedance is $Lg = 600\,uH$ and $Rg = 0.25\,\Omega$ and the system was tested under the inveter turn-off. For 13, the grid impedance is made by a RLC circuit, in which the capacitor is in parallel with the PCC. The values are $R_s = 25\,m\Omega$, $L_s = 480\,uH$ and $C_s = 46\,nF$. For both case, the parameters of the PR controller were kept unchanged. The inverter output current tracks the reference signal with excellent performance in these cases, indicating that the proposed methodology to design a digital PR controller is efficacy for LCL-filtered GCI even for the case where the the system is prone to have small grid impedance variations.

Fig. 14 presents a picture of the HIL experimental setup. The probes of the oscilloscope are connected on the analog outputs of the RTS. The microcontroller is connected on the interface board and its programming file is loaded through a USB debugger.

V. Conclusions

This paper presented a HIL verification of a LCL-filtered grid-connected inverter with digital PR current controller. The HIL setup was carefully described, indicating what runs within the RTS and what is executed in a microcontroller. The RTS and the microcontroller used were HIL402 and

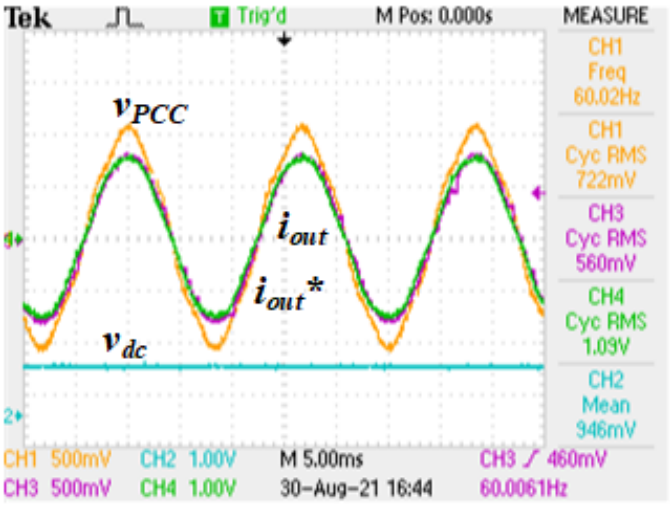

Fig. 11. steady-state behavior of the system when the PCC voltage has harmonic distortions.

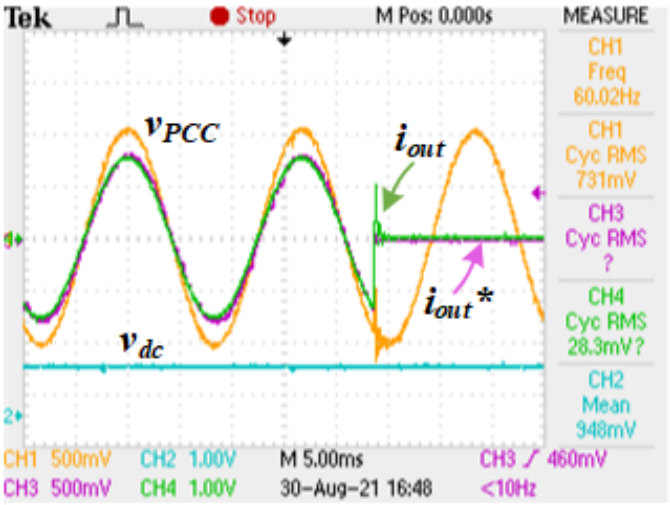

Fig. 12. Evaluation under different grid impedance and during the inverter turn-off.

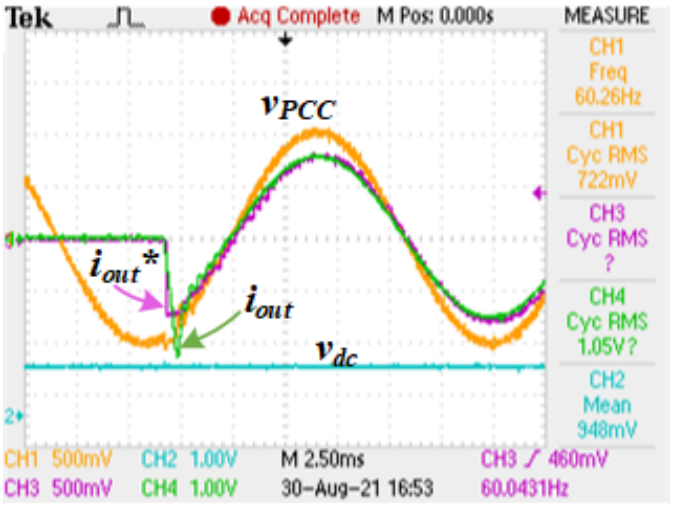

Fig. 13. Initialization when the grid impedance is made by RLC.

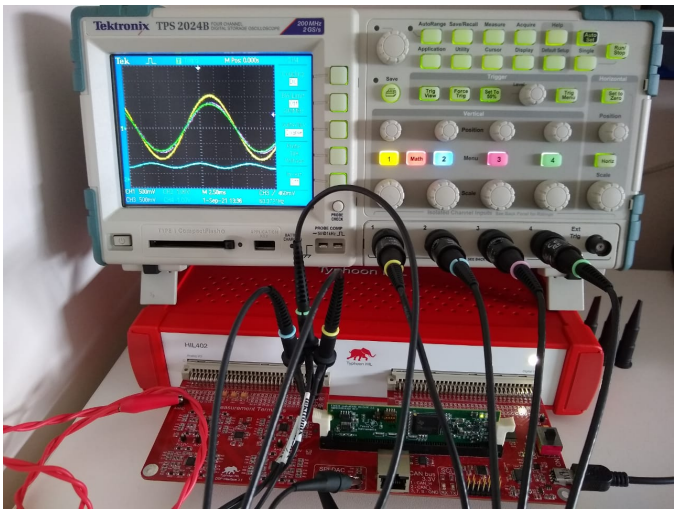

Fig. 14. Picture of the HIL experimental setup.

TMS320F28335, respectively. The design of the digital PR controller was given in a comprehensive manner, in which the output of the procedure was all the parameters of the controller. For the HIL experimental verification, changes were applied along the system like reference steps, inclusions of harmonics at the PCC, inclusion of oscillation at the DC-link and modification of the grid impedance. The inverter operated for all tests, indicating the accuracy of the designed PR controller. Results showed that the HIL experimental setup is an attractive tool for evaluating PR current controller of a LCL-filtered grid-connected inverter. The project files used in this research are freely available on the author's webpage http://busarello.prof.ufsc.br.

References

[1] M. D. Omar Faruque, T. Strasser, G. Lauss, *et al.*, "Real-Time Simulation Technologies for Power Systems Design, Testing, and Analysis," *IEEE Power and Energy Technology Systems Journal*, vol. 2, no. 2, pp. 63–73, Jun. 2015.

[2] S. Milovanovic, I. Polanco, M. Utvic, and D. Dujic, "Flexible and efficient mmc digital twin realized with small-scale real-time simulators," *IEEE Power Electronics Magazine*, vol. 8, no. 2, pp. 24–33, 2021.

[3] C. S. Goli, M. Manjrekar, P. Sahu, A. Chanda, and S. Essakiappan, "Implementation of stationary and synchronous frame current regulators for grid tied inverter using typhoon hardware in loop system," in *2021 IEEE 12th International Symposium on Power Electronics for Distributed Generation Systems (PEDG)*, 2021, pp. 1–8.

[4] E. Tremblay, A. Kachurowski, D. Leschert, and K. Busby, "Protective relay upgrade utilizing real-time simulator technology: Application in an industrial facility," *IEEE Industry Applications Magazine*, vol. 27, no. 4, pp. 57–68, 2021.

[5] R. Rajesh Kanna, R. Raja Singh, and D. Arun Dominic, "Impact analysis of single line to ground fault on industrial loads using typhoon hil," in *Innovations in Electrical and Electronic Engineering*, S. Mekhilef, M. Favorskaya, R. K. Pandey, and R. N. Shaw, Eds., Singapore: Springer Singapore, 2021, pp. 63–79.

[6] O. Adeosun, M. F. Rahman, E. Shoubaki, V. Cecchi, and M. Manjrekar, "Effect of inverter-interfaced distributed generation on negative sequence directional element using typhoon real-time hardware in the loop (hil)," in *2021 IEEE Applied Power Electronics Conference and Exposition (APEC)*, 2021, pp. 2097–2104.

[7] S. Dedeoglu, G. C. Konstantopoulos, and H. Komurcugil, "Current-limiting virtual synchronous control and stability analysis considering dc-link dynamics under normal and faulty grid conditions," *IEEE Journal of Emerging and Selected Topics in Power Electronics*, pp. 1–1, 2021.

[8] M. Nazir, J. H. Enslin, and K. Burkes, "Hybrid bypass protection of hybrid smart transformers for advanced grid support," in *2021 IEEE 12th International Symposium on Power Electronics for Distributed Generation Systems (PEDG)*, 2021, pp. 1–5.

[9] E. D. Queiroz, J. I. Y. Ota, and J. A. Pomilio, "Effect of pll on current distortion of droop-controlled converters in a control-in-the-loop simulation of a microgrid," in *2021 16th Brazilian Power Electronics Conference (COBEP) 2021, João Pessoa, Brazil*, 2021, pp. 1–6.

[10] F. Blaabjerg and D. M. Ionel, "Renewable energy devices and systems - state-of-the-art technology, research and development, challenges and future trends," *Taylor and Francis*, pp. 1319–1328, Jul. 2015.

[11] J. F. Guerreiro, D. I. Narváez, M. V. Gomes dos Reis, M. G. Villalva, and J. A. Pomilio, "Dynamic analysis of heterogeneous power converters operating in a droop-based microgrid," in *2017 IEEE 8th International Symposium on Power Electronics for Distributed Generation Systems (PEDG)*, 2017, pp. 1–8. DOI: 10.1109/PEDG.2017.7972510.

[12] S. U. Islam, K. Zeb, W. U. Din, *et al.*, "Design of a proportional resonant controller with resonant harmonic compensator and fault ride trough strategies for a grid-connected photovoltaic system," *Electronics*, vol. 7, no. 12, 2018.

[13] T. D. C. Busarello, J. A. Pomilio, and M. G. Simoes, "Design procedure for a digital proportional-resonant current controller in a grid connected inverter," in *2018 IEEE 4th Southern Power Electronics Conference (SPEC)*, 2018, pp. 1–8.

[14] O. Husev, C. Roncero-Clemente, E. Makovenko, S. P. Pimentel, D. Vinnikov, and J. Martins, "Optimization and implementation of the proportional-resonant controller for grid-connected inverter with significant computation delay," *IEEE Transactions on Industrial Electronics*, vol. 67, no. 2, pp. 1201–1211, 2020.

[15] G. R. Wehmuth, T. D. Curi Busarello, and A. Péres, "Step-by-step design procedure for lcl-type single-phase grid connected inverter using digital proportional-resonant controller with capacitor-current feedback," in *2021 IEEE Green Technologies Conference (GreenTech)*, 2021, pp. 448–454.

[16] J. F. Guerreiro, H. Guillardi Júnior, and J. A. Pomílio, "An approach to the design of stable distributed energy resources," in *2018 IEEE 19th Workshop on Control and Modeling for Power Electronics (COMPEL)*, 2018, pp. 1–8.

[17] J. F. Guerreiro, H. G. Júnior, J. I. Yutaka Ota, and J. A. Pomilio, "An enhanced thévenin equivalent circuit of a resonant-controller-based utility-interface," in *2019 IEEE 15th Brazilian Power Electronics Conference and 5th IEEE Southern Power Electronics Conference (COBEP/SPEC)*, 2019, pp. 1–6. DOI: 10.1109/COBEP/SPEC44138.2019.9065660.

[18] S. Bacha, I. Munteanu, and A. I. Bratcu, *Power Electronic Converters Modeling and Control: with Case Studies*, en. Springer Science & Business Media, Nov. 2013, ISBN: 978-1-4471-5478-5.

[19] F. Blaabjerg, *Control of Power Electronic Converters and Systems: Volume 2*, en. Academic Press, Apr. 2018, ISBN: 978-0-12-816168-5.

[20] T. D. C. Busarello, K. Zeb, A. Péres, V. S. R. V. Oruganti, and M. G. Simões, "Designing a second order generalized integrator digital phase locked loop based on a frequency response approach," in *2019 IEEE PES Innovative Smart Grid Technologies Conference - Latin America (ISGT Latin America)*, 2019, pp. 1–6.

[21] R. Teodorescu, M. Liserre, and P. Rodriguez, *Grid Converters for Photovoltaic and Wind Power Systems*, en. John Wiley & Sons, Jul. 2011, ISBN: 978-1-119-95720-1.

[22] A. V. Oppenheim, A. S. Willsky, S. H. Nawab, w. Hamid, and G. M. Hernández, *Signals & Systems*, es. Pearson Educación, 1997, ISBN: 978-970-17-0116-4.

[23] T. D. Curi Busarello, K. Zeb, and M. G. Simões, "Highly accurate digital current controllers for single-phase lcl-filtered grid-connected inverters," *Electricity*, vol. 1, no. 1, pp. 12–36, 2020.